Water Propagation on a Surface with Buried Nanochannels

CNF Project Number: 2123-12

Principal Investigator(s): Shalabh C. Maroo

User(s): Sajag Poudel, An Zou, Manish Gupta

Affiliation(s): Department of Mechanical and Aerospace Engineering, Syracuse University, Syracuse, NY 13244

Primary Source(s) of Research Funding: National Science Foundation Career Award NO. 1454450, Office of Naval Research Grant NO. N000141812357

Contact: scmaroo@syr.edu, sapoudel@syr.edu, azou@syr.edu, magupta@syr.edu

Website: http://maroo.syr.edu

Primary CNF Tools Used: Heidelberg mask writer (DWL 2000), manual photoresist spinner, Gamma coat-develop tool, GCA auto stepper, ASML stepper, YES image reversal oven, ABM contact aligner, SÜSS MA6-BA6 contact aligner, e-beam evaporator, Oxford PECVD, GSI PECVD, Glen 1000 Plasma, Anatech resist strip, Oxford 81/82 etcher, Oxford 100 etcher, Plasma-Therm deep silicon etcher, Unaxis 770 deep silicon etcher, optical microscope, scanning electron microscope, atomic force microscope

Abstract:

We investigated the wicking of a finite water drop sitting on a surface with well-defined cross-connected buried nanochannels by experiments and analytical models. The wicking process is composed of wicking-dominant and evaporation-dominant regimes, with each further divided into two subregimes. The wicking is initially governed by surface tension and viscous forces, and later by hydrodynamic dissipation within the droplet sitting on the top surface due to the finite liquid supply. The work reported here is part of a journal article published in Journal of Physical Chemistry C [1].

Summary of Research:

Wicking is the phenomenon in which liquid propagates in a porous medium primarily due to the surface tension, curvature, and the solid-liquid intermolecular attraction force. Wicking plays a significant role in various areas, such as thin film evaporation, printing, oil processing, etc. Superior wickability of a porous medium is a major motivation to employ them in phase-change heat transfer applications, which is widely accepted as one of the most promising solutions to the increasing demand of high heat flux removal. Here, we present an experimental work of water propagation on a surface with buried nanochannels. The geometry of the nanochannel being well controlled and defined makes it a perfect candidate to conduct such investigation due to: (1) accurately modeled capillary pressure without having to predict the meniscus shape; and (2) easily achieved long wicking distance as the evaporation is hindered.

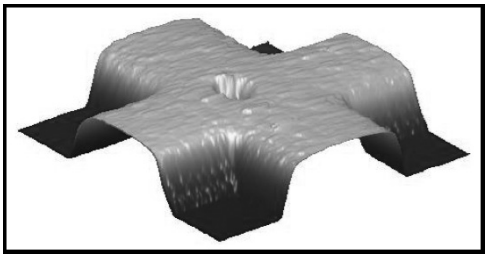

Figure 1: Atomic force microscope (AFM) image of the profile of channels and pores.

The buried cross-connected nanochannels were fabricated on a silicon (Si) substrate by etching patterned sacrificial metal layers buried under a 300 nm thick silicon dioxide (SiO_2) film from plasma enhanced chemical vapor deposition (PECVD). The channel geometry was determined by the pattern of sacrificial layers, which was attained by a lift-off process. The cross-connected channels, made from two sets of channels perpendicular to each other, allow for ease of liquid exchange inside the channels. Further, at each intersect of the channels, a 2 μm pore was fabricated allowing liquid present above the surface to flow into the channels. Figure 1 shows an atomic force microscope (AFM) image of the surface (channel width: 5 μm, spacing: 5 μm, height: 728 nm).

In wicking experiments, the spreading of a 2-μL water droplet on a sample with buried nanochannels was recorded using a high speed camera. The volume of the droplet was generated and controlled by a string pump. Using a vertical-translation stage, the sample was raised until it touched the droplet, after which the droplet starts to spread on the surface, as well as wick into the channels before eventually drying out due to evaporation. The water propagation during wicking were characterized by three parameters: wicking radius

(R_w, defined as radius of the entire wetted area), droplet base radius (R_d, defined as radius of the droplet sitting above nanochannels), and wicking distance (w_d, defined as difference between above two). Figure 2 shows a schematic of these parameters. Both R_w and R_d were obtained from image analysis of the high-speed video and were measured with time.

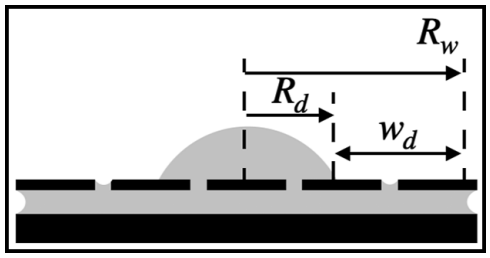

Figure 2: Schematic of definition of wicking radius (R_w) and droplet base radius (R_d).

Figure 3 shows the evolution of R_w and R_d. The wicking process can be divided into two distinct regimes: initial wicking-dominate (regime I) and later evaporation-dominant regime (II). Each of these two regimes can be further divided into two subregimes. When the droplet comes in contact with the surface (defined as t = 0), it spreads on the top of the surface immediately; water starts wicking into the channels as well, causing both R_d and R_w to increase fast in the first subregime I-A. The end of subregime I-A is defined by the time ($t = t_d$) when R_d reaches its maximum. In subregime I-B, the water menisci in the channels continues to advance radially outward and reaches a maximum wicking radius at $t = t_{max}$; while the R_w remains nearly constant during this period. Beyond t_{max}, the wicking process transitions to regime II where evaporation dominates, causing the meniscus front recede and dry out eventually due to the finite water supply from the droplet.

In subregime II-A, the water evaporated from menisci in the channels and pores is balanced by the water supply from the droplet, leading to a nearly constant R_w. The R_d maintains at its maximum as well, with a decrease in droplet height due to the shrink in volume. After the droplet height reaches a certain minimum value, water front above nanochannels starts to recede, leading to a decreased R_d and therefore subregime II-B where evaporation flux in menisci in channels overwhelms water supply from the droplet, causing R_w to decrease and eventually dry out.

The data of wicking distance (w_d) in regime I are in good agreement with two analytical models which can be used to predict wicking distance evolution in nanochannels. In regime I-A, the w_d can be predicted by Xiao's model [2] where the flow is governed by surface tension (flow driving force) and viscous forces (flow resistance) with unlimited liquid supply. Due to the finite droplet volume, the w_d deviates from this prediction in regime I-B, but is in good agreement with prediction from Ruijter's model [3], where the hydrodynamic dissipation within droplet was considered as the dominant reason behind the loss of surface during spreading.

Conclusions and Future Steps:

The wicking in buried nanochannels is composed of wicking-dominant and evaporation-dominant regimes. The wicking is initially governed by surface tension and viscous forces, and later by hydrodynamic dissipation within the droplet sitting on the top surface.

References:

[1] S. Poudel, A. Zou, S.C. Maroo, J. Phys. Chem. C, 123: 23529-23534 (2019).

[2] R. Xiao, R. Enright, E.N. Wang, Langmuir, 26: 15070-075 (2010).

[3] M.J. de Ruijter, J. De Coninck, G. Oshanin, Langmuir, 15: 2209-2216 (1999).

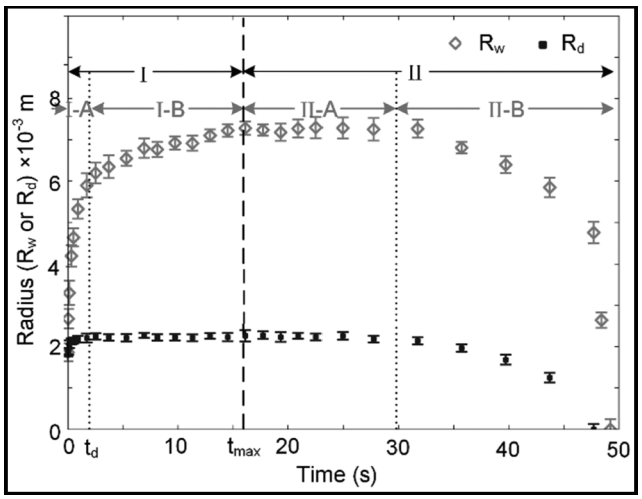

Figure 3: Evolution of wicking radius (R_w) and droplet base radius (R_d) for wicking of 2 μl droplet.